Bannuscher, A., **Karkossa, I.**, Buhs, S., Nollau, P., Kettler, K., Balas, M., Dinischiotu, A., Hellack, B., Wiemann, M., Luch, A., **von Bergen, M.**, Haase, A., **Schubert, K.** (2020):
A multi-omics approach reveals mechanisms of nanomaterial toxicity and structure–activity relationships in alveolar macrophages
Nanotoxicology **14** (2), 181 - 195

http://dx.doi.org/10.1080/17435390.2019.1684592

A Multi-Omics Approach Reveals Mechanisms of Nanomaterial Toxicity and Structure-Activity-Relationships in Alveolar Macrophages

Anne Bannuscher*[a], Isabel Karkossa*[b], Sophia Buhs[c], Peter Nollau[c], Katja Kettler[a], Mihaela Balas[d], Anca Dinischiotu[d], Bryan Hellack[e,f], Martin Wiemann[g], Andreas Luch[a], Martin von Bergen[b,h], Andrea Haase*[a], Kristin Schubert*[b]

[a] Department of Chemical and Product Safety, German Federal Institute for Risk Assessment (BfR), Max-Dohrn-Straße 8-10, 10589 Berlin, Germany

[b] Department of Molecular Systems Biology, UFZ, Helmholtz-Centre for Environmental Research, Permoserstraße 15, 04318 Leipzig, Germany

[c] Research Institute Children's Cancer Center and Department of Pediatric Hematology and Oncology, University Medical Center Hamburg-Eppendorf, Hamburg, Germany

[d] Department of Biochemistry and Molecular Biology, Faculty of Biology, University of Bucharest, 91-95 Splaiul Independentei, 050095, Bucharest, Romania

[e] Institute of Energy and Environmental Technology (IUTA) e.V., Duisburg, Germany

[f] German Environment Agency, Dessau, Germany

[g] IBE R&D gGmbH Institute for Lung Health, Mendelstraße 11, 48149, Münster, Germany

[h] Institute of Biochemistry, Leipzig University, Brüderstraße 34, 04103 Leipzig, Germany

* These authors contributed equally

Corresponding author:

Kristin Schubert

E-Mail: kristin.schubert@ufz.de

Telephone: +49 341 235 1211

Keywords:

Nanomaterials, Proteomics, Metabolomics, SH2 profiling, Multi-Omics, WGCNA, Alveolar Macrophages

Supplementary Material:

The Supplementary Material contains mainly raw data.

Abstract

In respect to the high number of released nanomaterials and their highly variable properties, novel grouping approaches are required based on the effects of nanomaterials. Proper grouping calls for a combination of an experimental setup with a higher number of structurally similar nanomaterials and for employing integrated omics approaches to identify the mode of action.

Here we analyzed the effects of seven well characterized NMs comprising different chemical compositions, sizes and chemical surface modifications on the rat alveolar macrophage cell line NR8383. The NMs were investigated at three doses ranging from 2.5 - 10 µg/cm^2 after 24 h incubation using an integrated multi-omics approach involving untargeted proteomics, targeted metabolomics and src homology 2 (SH2) profiling. By using Weighted Gene Correlation Network Analysis (WGCNA) for the integrative data, we identified correlations of molecular pathways with physico-chemical properties and toxicological endpoints. The three investigated SiO2 variants induced strong alterations in all three omics approaches and were therefore be classified as ”active”. Two organic phthalocyanines showed minor responses and Mn2O3 induced a different molecular response pattern than the other NMs. WGCNA revealed that agglomerate size and surface area as well as LDH release are among the most important parameters correlating with nanotoxicology. Moreover, we identified key drivers that can serve as representative biomarker candidates, supporting the value of multi-omics approaches to establish integrated approaches to testing and assessment (IATAs).

Introduction

Due to their specific and often unique properties nanomaterials (NMs) are applied in a wide range of different applications (Stark *et al.*, 2015) and physico-chemical properties of NMs can be fine-tuned resulting in a broad range of NM variants. However, altering size, shape, morphology and surface chemistry of a NM may modify its biologic interactions, activity and/or biokinetics (Landsiedel *et al.*, 2012, Arts *et al.*, 2015, Louro, 2018), thus influencing the potential toxicity (Oberdörster *et al.*, 2005, Rahi *et al.*, 2014).

In the last decades, nanosafety research has generated a huge amount of studies describing potential NM hazards *in vitro*. These have increased our general understanding of nanotoxicity but are of limited relevance for risk assessment (Krug, 2014). Regulatory risk assessment of chemicals including NMs still mainly depends on *in vivo* testing to fulfill information requirements, even though animal tests are time-consuming, costly and ethically questionable. In addition, there are debates on whether the underlying mechanisms are conserved between species (Olson *et al.*, 2000, Wall and Shani, 2008, Shanks *et al.*, 2009). Unfortunately, it is neither easy nor straightforward to replace animal tests by *in vitro* assays. The current state-of-the art is to develop integrated approaches to testing and assessment (IATAs) combining several *in chemico*, *in vitro* and *in vivo* tests in a structured manner employing specific decision trees (OECD, 2018). For this purpose the inclusion of mechanism-linked bioactivity assays along with traditional cytotoxicity assays for *in vitro* screening as well as the correlation of toxicity effects with physico-chemical properties has been shown to be advantageous (Xia *et al.*, 2013, Feliu *et al.*, 2016). Furthermore, the development of IATAs is strongly connected to the development of Adverse Outcome Pathways (AOPs) (OECD, 2012).

The development of IATAs and AOPs for NMs has made great progress recently (Shatkin and Ong, 2016, Gerloff *et al.*, 2017). However, it is hampered by a still limited understanding of NM toxicity mechanisms and mode of actions (MoAs). A few MoAs concerning some toxicological endpoints of some NMs are already quite well understood. Examples are the release of toxic ions for some metal and metal oxide NMs, the fibre paradigm following inhalation of bio-persistent high aspect ratio NMs, and the generation of oxidative stress due to a highly specific surface area and/or surface reactivity (Donaldson *et al.*, 2006, Nel *et al.*, 2006, McShan *et al.*, 2014, Arts *et al.*, 2015, Dong and Ma, 2015, Tee *et al.*, 2016). However, for many NMs the underlying MoAs are not well understood but toxicogenomics techniques have been shown to be in particular useful to elucidate NM toxicity mechanisms and MoAs (Lin *et al.*, 2013, Riebeling *et al.*, 2017). Furthermore, there are several studies that used a single omics technique to understand molecular changes induced by NMs (Nath Roy *et al.*, 2017). However, each technique individually provides only limited insights into the overall appearance which was demonstrated in a multi-omics study conducted with ten different CNTs (Scala *et al.*, 2018). Thus, the number of studies using complementary omics approaches is increasing (Scala *et al.*, 2018, Gallud *et al.*, 2019), where often transcriptomics and proteomics have been combined, while posttranslational modifications or metabolomics have been included less frequently.

Here we applied a multi-omics approach comprising untargeted proteomics, targeted metabolomics and SH2 profiling to investigate the effects of seven NMs in an alveolar macrophage cell line (NR8383). The chosen NMs possess different chemical compositions, sizes, shapes and surface chemistries and have been extensively characterized. Moreover, most of them were already well characterized with respect to their inhalation toxicity by *in vivo* short-term inhalation studies (STIS) and standard *in vitro* assays in the same cellular model (Wiemann *et al.*, 2016). Hence,

plenty of existing toxicological and physico-chemical data are available for correlation with our multi-omics approach. For this purpose Weighted Gene Correlation Network Analysis (WGCNA), a p-value independent co-expression network approach, was used (Zhang and Horvath, 2005). WGCNA has been shown to be a valuable tool in systematically deciphering cellular responses or identifying pathways relevant to key traits or conditions (Pei *et al.*, 2017). Additionally, this type of analysis allows the correlation with external conditions or sample traits as for example physico-chemical properties (Langfelder and Horvath, 2008). Thus, we characterized not only NM specific effects on proteome and metabolome but also effects linked to physico-chemical properties.

Materials and Methods

Selected NMs and NM characterization

A set of seven NMs with specifically selected properties was investigated. Unmodified SiO2_15 (precipitated) was provided by BASF SE. Phthalocyanine Blue and Phthalocyanine Green were provided by BASF Colors and Effects in technical grade. SiO2_7 (pyrogenic) and SiO2_40 (pyrogenic) were manufactured by Evonik Industries. Graphene Oxide was obtained from Sigma-Aldrich. All NMs were delivered as powders, except SiO2_15, which was provided in suspension. The supplement contains a description of the NMs physico-chemical properties (Table S1) and average values in F12K cell culture medium (Table S2 - Table S4). Selected properties are summarized in Table 1.

NM Dispersion

NMs were dispersed freshly prior use by an indirect probe sonication protocol with a Bandelin Cup Horn (Bandelin, Germany). A 0.5 mg/ml stock solution was prepared in water or serum-free cell culture medium. The centrifuge vial was placed in the middle of the Cup Horn or in a multi-vial holder and sonicated to a final power input of 6 W during continuous water exchange (Taurozzi *et al.*, 2011).

NM Characterization

For the basic physical chemical characterization the NMs were suspended in deionized water (0.5 mg/ml) and in various cell media (F12K and DMEM plus Fetal Calf Serum) and analyzed by different techniques (or data were given by literature or provider) towards their primary particle size (Scanning Electron Microscopy – SEM, Brunauer-Emmett-Teller – BET), agglomeration size

(SEM, Dynamic Light Scattering – DLS), specific surface area (BET, DLS, SEM), pH-dependent zeta potential (Electrophoretic Light Scattering - ELS), isoelectric point (ELS), pH value & redox potential (Electrodes), oxidative potential (spin trap and spin probe based EPR spectroscopy), solubility/dissolution (in a steady state system after 24 h and 48 h shaking by Inductive Coupled Plasma Optical Emission Spectrometry - ICP-OES), morphology (SEM), density (literature) and band gap (Ultraviolet-Visible spectroscopy - UV/VIS). Dispersion and analysis were performed according to former NM characterization procedures published by nanOxiMet, nanoGEM, MARINA. Slight adjustments to NanoToxClass NM characterization can be found in specific SOPs (www.nanotoxclass.eu).

Cell culture

NR8383 alveolar macrophages (ATCC, CRL-2192, USA) were cultivated in Ham's F12K medium (Thermo Fisher Scientific, #21127030, USA), supplemented with 15 % FCS (heat-inactivated, PAN Biotech, P30-1506, Germany), 100 U/mL penicillin and 100 µg/mL streptomycin (PAN Biotech, P06-07100, Germany). Cells were exposed to 45, 22.5 and 11.25 µg/mL NM for 24 h under serum free conditions. Thus, nominal doses assuming complete sedimentation were 10, 5 and 2.5 µg/cm^2.

In vitro toxicity

Cytotoxicty of NMs was assessed by lactate dehydrogenase (LDH) and β-glucuronidase (GLU) release. In addition, H_2O_2 formation and tumor necrosis factor alpha (TNFα) release were investigated. Information were taken from literature, if available (Wiemann *et al.*, 2016). For the remaining NMs, toxicity was investigated using the same methods as described before (Wiemann

et al., 2016) with one exception. TNFα levels were determined by ELISA (BMS622, Thermo Fisher Scientific, Austria), following manufacturer's instructions.

For the H_2O_2 assay NR8383 cells were seeded at a density of 5×10^5 cells/ml in 96-well plates and were exposed to NMs in serum free Ham's F12K medium for 16 h, and 1.5 h. Blanks (cell free medium ± NMs) corresponding to each sample were used to eliminate any interference. Three biological replicates from each sample were acquired using a FlexStation 3 multiplate reader (Molecular Devices, San Jose, CA). The obtained values are summarized in Table S9 for NM screening and in Table S10 for concentration-dependent effects.

Sample Preparation for Omics Studies

Cells (4×10^6) were seeded in complete cell culture medium into 22 cm^2 cell culture dishes (TPP, Switzerland) and rested overnight. Freshly dispersed NMs were added, followed by incubation for 24 h in serum-free medium. For the initial screening NMs were applied at 10 µg/cm^2, which corresponds to *in vivo* overload conditions in rat lungs (Kroll *et al.*, 2011). Protein samples were generated in three to five biological replicates, containing untreated control samples, while metabolites were extracted from four to six replicates. Dose-dependent effects were investigated for selected NMs at doses of 2.5, 5 and 10 µg/cm^2 with three to four biological replicates. Detailed information can be revealed from Additional file 1. Proteins and metabolites were extracted from individual samples prepared at the same day.

Proteins for proteomics and SH2 profiling were extracted from the same samples using RIPA buffer containing 0.05 M Tris/ HCl (pH 7.4, Roth, Germany), 0.15 M Na-chloride (Roth, Germany), 0.001 M EDTA (Roth, Germany), 1 % Igepal (Sigma Aldrich, Germany), 0.25 % Na-deoxycholate (Sigma Aldrich, Germany), 10 mM Na-Pyrophosphate (Sigma Aldrich, Germany),

10 mM β-Glycerolphosphate (Sigma Aldrich, Germany), 1 mM Na-orthovanadate (Sigma Aldrich, Germany), 10 µl/ml Protease-inhibitor (Merck Millipore, USA), 10 µl/ml β-Mercaptoethanol, 10 µl/ml Na-fluoride and 2 µl/ml Na-pervanadate. Protein concentrations were determined using Bradford assay (Bio-Rad, USA). Metabolites were extracted using 5 % (v/v) chloroform, 45 % (v/v) methanol, 50 % (v/v) water.

Targeted Metabolomics, untargeted Proteomics and SH2 profiling

For Metabolomics, the AbsoluteIDQ p180 Kit (Biocrates, Austria) was used as described previously (Potratz *et al.*, 2017). Samples were analyzed with an API 5500 triple quadrupole mass spectrometer (ABSciex, Germany) coupled to an Agilent 1260 Infinity HPLC system (Agilent, USA). Analyst® software and MetIDQ were used for data analysis. Values below the limit of detection were excluded. Fold changes (FCs, treatment vs. control) were calculated prior further analysis.

For proteomics, tandem mass tag (TMT)-labeling (TMT-10-plex, Thermo Scientific, USA) was applied. In case of the screening the workflow was as specified in manufacturer's instructions and as described before but with 50 µg protein (Thompson *et al.*, 2003, Wewering *et al.*, 2016). For the investigation of dose-dependent effects, TMT labeling was performed on paramagnetic beads (Supplement: Using tandem mass tags on paramagnetic beads), which leads to an improved sample quality and allows for fractionation (Hughes *et al.*, 2014, Hughes *et al.*, 2018).

In both cases, labeled samples obtained from one biological replicate were combined and analyzed on a nano-UPLC system (Ultimate 3000, Dionex, USA). After trapping (Acclaim PepMap 100 C18, 3 µm, nanoViper, 75 µm × 5 cm, Thermo Fisher, Germany), peptides were separated on a reversed-phase column (Acclaim PepMap 100 C18, 3 µm, nanoViper, 75 µm × 25 cm, Thermo

Fisher, Germany), applying a non-linear gradient of 150 minutes. Obtained MS raw data were processed using ProteomeDiscoverer 2.1.0.81, where we applied a co-isolation threshold of 50 % to minimize ratio compressions (Sandberg et al., 2014). The database search was performed against the UniprotKB reference proteome of rattus norvegicus (28 April 2017), resulting in FCs (treatment vs. control) for 2051 proteins, which were log2-transformed and median normalized before further analyses.

SH2 profiling was performed as described previously (Dierck *et al.*, 2009). In brief, RIPA extracts were separated by SDS-PAGE, transferred to PVDF membranes, blocked with 10% skim milk in TBST buffer and probed with different SH2-domains pre-complexed with streptavidin/horseradish-peroxidase conjugate. Tyrosine phosphorylated proteins were detected by chemiluminescence, films were scanned and signal intensities of individual phosphoprotein bands were quantified applying ImageJ software package. Mean signal intensities of phosphoprotein bands were calculated from minimum three (to five) biological replicates and FCs of phosphorylation were determined in comparison to mean signals obtained from controls.

Statistical Analysis

Statistical analysis of the log2-transformed FCs was performed in R-3.5.0. To unravel significant (p-value ≤ 0.05) changes compared to control, the Student's t-test with Benjamini & Hochberg adjustment was performed for proteins and metabolites that were quantified in at least three biological replicates over all the treatments. Hierarchical clustering was conducted with Euclidean distance measure and complete clustering algorithm. FCs and adjusted p-values for all data sets can be found in Additional file 1.

Integrative Analysis

For integrative analysis, Log2(FCs) of all proteins and metabolites obtained in the initial screening with seven NMs (independently of the p-value) were scaled to integer values between 0 and 100, without changing the distribution of the values per sample (Additional file 2) (Langfelder and Horvath, 2008, Love *et al.*, 2014).

Soft power in WGCNA was set to 18, cut-height to 0.1 and minimum module size to 25. 10 modules of co-expressed analytes were obtained (Figure S2). A summary of analytes that have been assigned to each of the modules can be found in Additional file 3. For each of the obtained modules significantly enriched pathways were determined using Ingenuity Pathway Analysis (IPA, Qiagen, Germany).

Results

NM characterization

NMs have been characterized extensively. Key physico-chemical properties are summarized in Table 1. More details are given in Table S1 - Table S4. Characterizations of several materials have also been published elsewhere (Landsiedel *et al.*, 2014, Driessen *et al.*, 2015, Wiemann *et al.*, 2016).

Table 1: Summary of physico-chemical properties.
Summarized are core materials, provided primary particle sizes (PPS) determined using BET, the agglomerate sizes in F12K determined using DLS as well as the zeta potential at pH 7.4. *(Wiemann *et al.*, 2016, Wiemann *et al.*, 2018)

Substance (CAS Nr.)	**Short Name**	**PPS (provided)**	**PPS (BET)**	**Agglomerate Size in F12K (z.average)**	**Zeta Potential**	**Name in Literature***
		[nm]	[m^2/g]	[nm]	[mV]	
Silica (7631-86-9)	**SiO2_15**	15	-	42.2 ± 5.4	-35.5 ± 3.6	SiO2.naked
	SiO2_40	40	66.2 ± 1.0	255.0 ± 2.1	-38.8 ± 19.4	F1
	SiO2_7	8	9.1 ± 0.2	275.1 ± 7.6	-26.6 ± 1.2	
Graphene Oxide	**Graphene Oxide**	NA	15.1 ± 0.1	1927.2 ± 594.4	-16.2 ± 10.9	
Cu-phathalo-cyanine (147-14-8)	**Phthalocyanine Blue**	17	75.6 ± 0.4	1760.1 ± 27.2	-24.1 ± 3.4	Pigment blue 15:1
Halogenated Cu-phathalo-cyanine (14832-14-5)	**Phthalocyanine Green**	NA	45.6 ± 0.1	1783.9 ± 304.1	-37.0 ± 4.3	
Manganese	**Mn2O3**	50	22.9 ± 0.1	675.6 ± 71.4	-24.6	

Proteomics, SH2 Profiling and Metabolomics

To get mechanistic information about NM effects on alveolar macrophages (NR8383) at a dose of 10 µg/cm^2, a multi-omics approach was applied. From proteomics, fold changes (FCs) of protein abundances relative to the control were obtained for 1200 proteins. Hierarchical clustering of protein FCs that is shown in Figure 1A revealed two groups of NMs: Silica NMs SiO2_7, SiO2_15 and SiO2_40 led to significant (p-value $\leq$ 0.05) changes in the proteome (Figure 1B), while Phthalocyanine Blue, Phthalocyanine Green, Mn2O3 and Graphene Oxide showed almost no significant alterations. SiO2_7 had a similar pattern as SiO2_15 and SiO2_40 but with considerably more significant changes. Thus, the silica NMs were classified to be "active".

SH2 profiling was performed to gain insights into changes of the global state of tyrosine phosphorylation after NM treatment. Profiling was performed with 11 different SH2 domains and the mean phosphoactivity of 648 phosphoprotein bands was determined (Figure S1). Clustering of the SH2 profiles revealed two major groups, in which SiO2_40, Mn2O3 and SiO2_15 were clearly separated from phthalocyanines and Graphene Oxide, while SiO2_7 was apart (Figure 1C). Significant (p-value $\leq$ 0.05) changes in the phosphorylation state of different proteins are summarized in Figure 1D, demonstrating that SiO2_7, SiO2_15 and SiO2_40 as well as Mn2O3 are among the top scorers leading to a strong decrease in tyrosine phosphorylation, while treatment by phthalocyanines and Graphene Oxide led to only few changes. Based on these findings, Mn2O3 and the three silica NMs tested here were classified to be "active".

The hierarchical clustering of metabolome data showed again the formation of three major clusters: SiO2_15 and SiO2_40 on the one hand and Phthalocyanine Blue, Phthalocyanine Green, Mn2O3 and Graphene Oxide on the other hand. SiO2_7 was separated from the other silica NMs due to its

considerably different expression profile (Figure 1E). Anyway, the comparison of significantly (p-value ≤ 0.05) altered metabolites (Figure 1F) highlights that SiO2_7, SiO2_15 and SiO2_40 are the NMs which induced significant changes, rendering these again as "active".

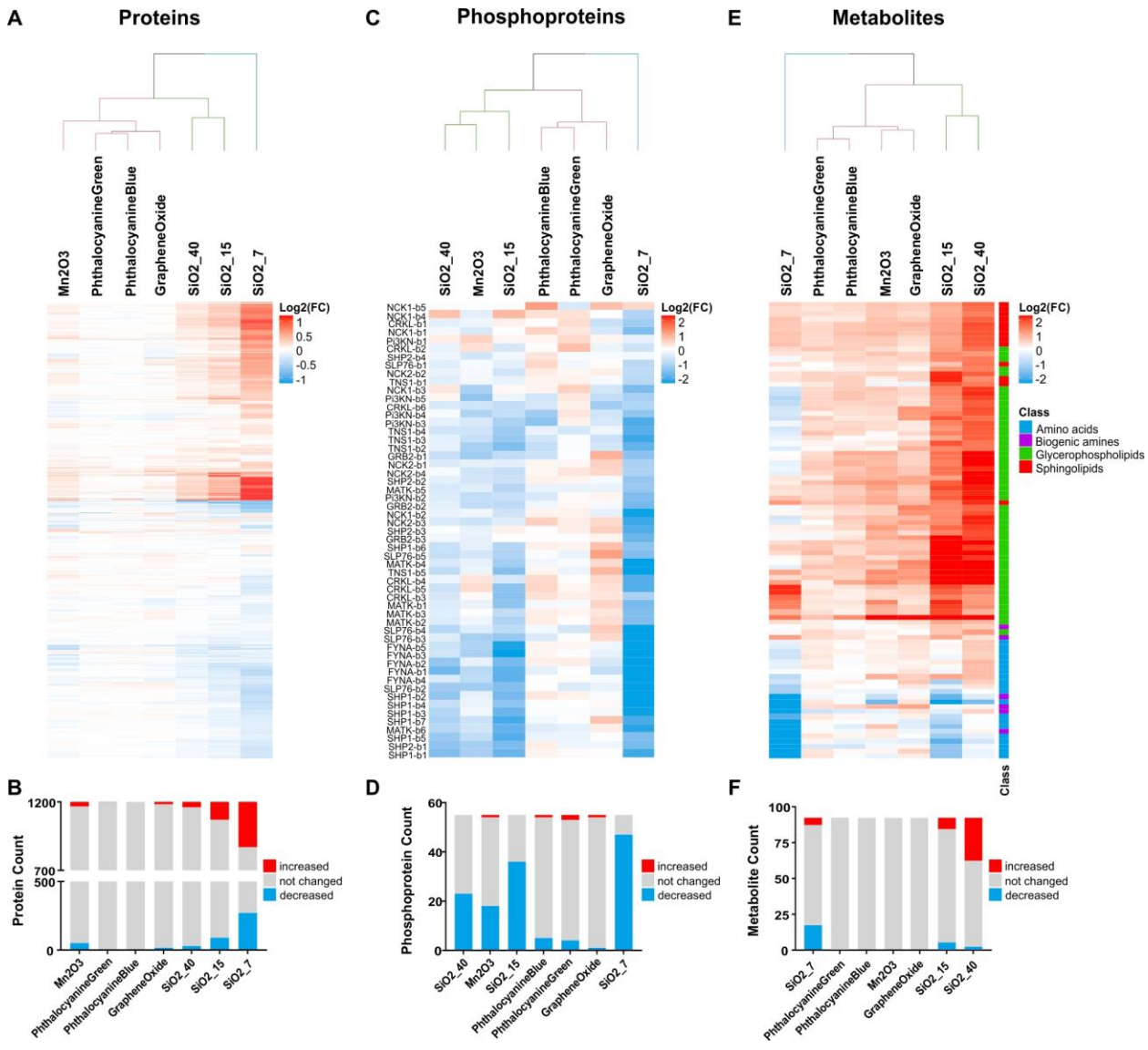

Figure 1: Summary of obtained proteins, phosphoproteins and metabolites.
Presented are Euclidean clustering analyses for proteins, phosphoproteins and metabolites in A, C and E, respectively, that are colored by Log2(FCs). B, D and F show numbers of analytes with significantly (p-value ≤ 0.05) altered abundances.

Next, we performed an integrated data evaluation, for which the data from proteome, phosphoproteome and metabolome at NM doses of 10 µg/cm^2 were scaled to the same range from

-2 to 2. Noticeably, the overall clustering remained the same (Figure 2). Again, SiO2_7 was located in a different cluster, pointing to a different MoA compared to SiO2_15 and SiO2_40. Since Mn2O3 is located in the middle of both clusters, we classified this NM as equivocal. The fact that the clusters derived from each individual method were highly comparable to the integrated clusters demonstrates that the gained multi-omics results are consistent.

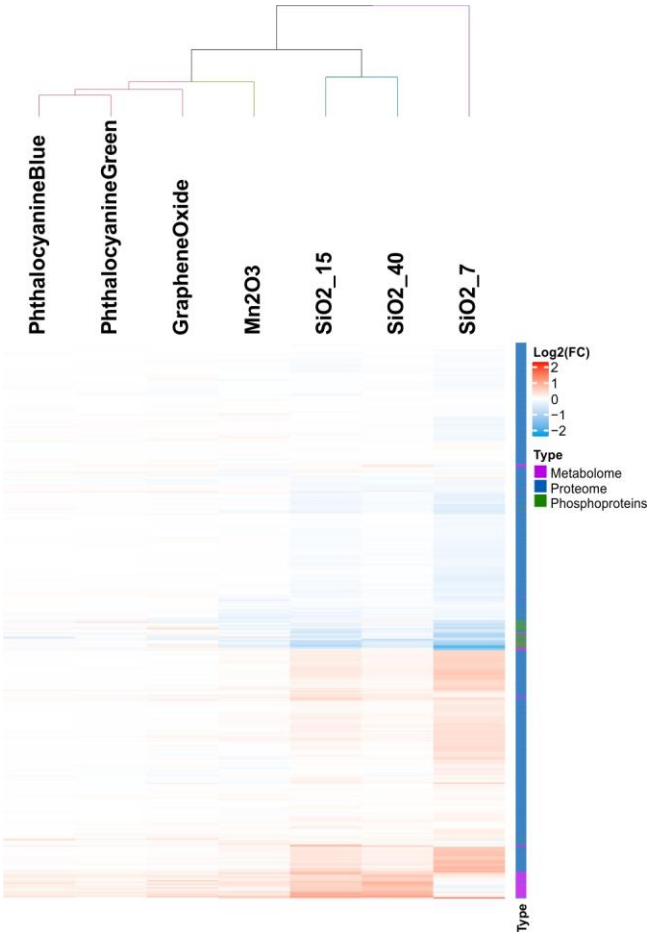

Figure 2: Results from integrative hierarchical clustering analysis.
Presented is a Euclidean clustering analysis conducted with protein, phosphoprotein and metabolite Log2(FCs) scaled to the same ranges (min = -2, max = 2). Coloring was performed based on the scaled Log2(FCs).

Integrative Analysis

To get information about the NMs MoAs and on physico-chemical properties influencing biological effects, we performed a WGCNA of proteins and metabolites. Co-expressed analytes were summarized into color-coded modules, followed by correlation of the obtained module eigengenes (modules first principal components) with traits (summarized in Table S5 - Table S9). WGCNA revealed ten modules which were analyzed by Ingenuity Pathway Analysis (IPA). A summary of WGCNA and IPA is provided in Table S11. Significant correlations with NM treatments were observed for SiO2_7, SiO2_15, SiO2_40, Mn2O3 and Phthalocyanine Blue (Figure 3A). Interestingly, the only but clearly significant correlation of Mn2O3 was associated with DNA methylation, Guanosine Nucleotides Degradation and Glycolysis indicating that Mn2O3 led to different cellular effects than the other tested NMs. Again, Mn2O3 was located in the middle of both trees (Fig. 3A). The significant correlations of the NM treatments with several of the modules and comprised pathways (Table S11) were analogous to the correlation patterns observed for the respective core materials and morphologies (Figure 3B, C). Furthermore, the clustering (Fig. 3A) was identical to the single omics analyses. Graphene Oxide and both phthalocyanines showed similarities although they are chemically different. The involved modules contained analytes linked to chemokine signaling, oxidative stress response and cell death (Table S11). In contrast, all silica variants showed negative correlations with the yellow module, which is positively associated with Mn2O3, Graphene Oxide and the phthalocyanines, promoting the assumption of different MoAs. Mn2O3 and SiO2_7 were clearly separated from the other two, but furthest apart. However, SiO2_15 and SiO2_40 were both positively correlating with the brown module, containing analytes connected to NRF2-mediated oxidative stress response and IL-8

297 signaling. SiO2_7 was the only NM significantly correlating with the turquoise module, containing
298 analytes related to mitochondrial dysfunction and DNA damage response.

299 Significant correlations of modules with physico-chemical properties and toxicological endpoints
300 (Figure 3D) were observable for agglomerate size and LDH release. These were anti-correlating,
301 indicating larger agglomerate forming NMs to lead to lower LDH release and concludingly to
302 higher cell viability. Results for agglomerates surface areas (SA (z.average)), DMPO reactivity,
303 band gap and TNFα release were analyzed in more detail below.
304

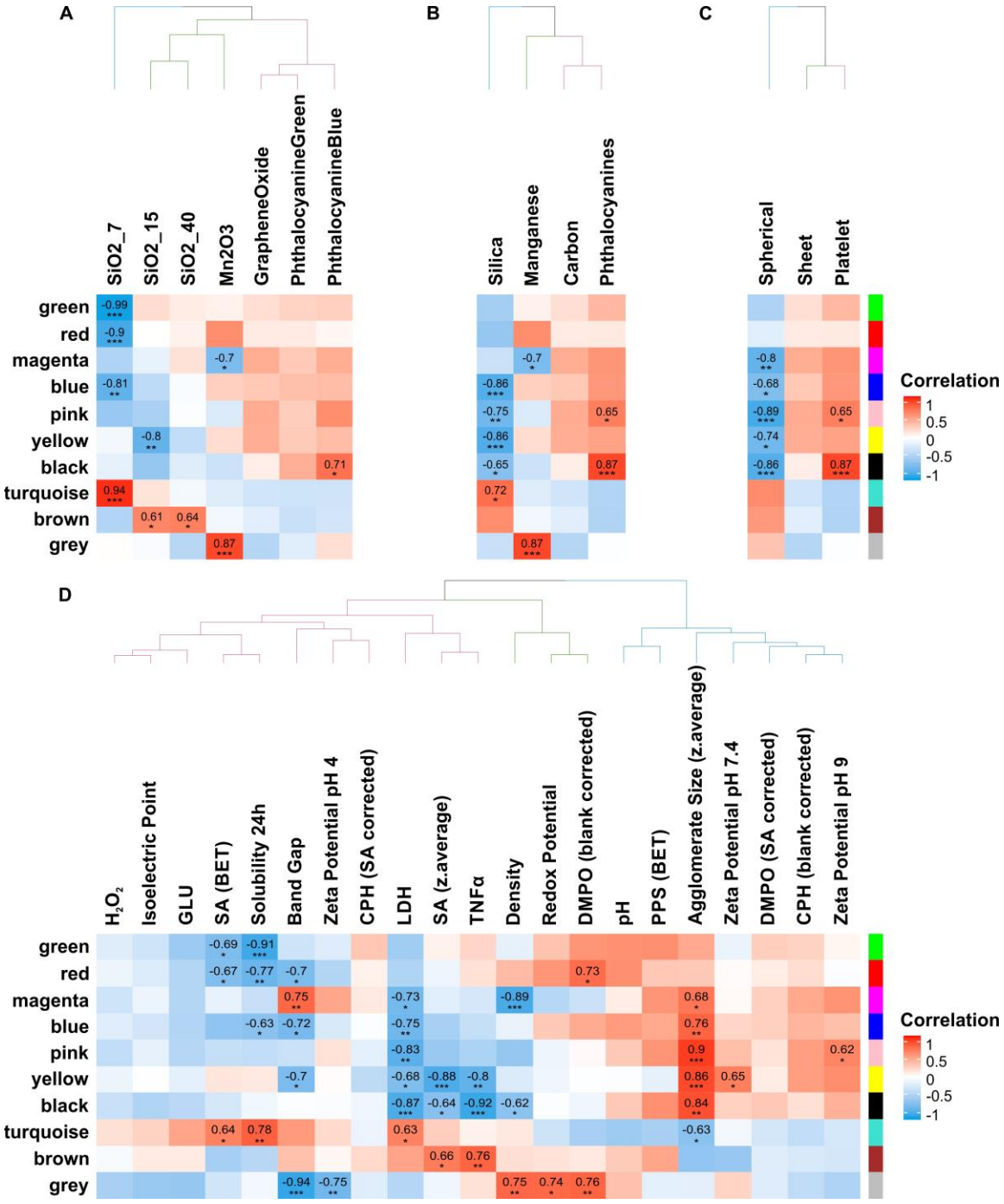

Figure 3: Results from module-trait correlation performed for WGCNA.
Shown are modules of co-expressed analytes that were correlated with NM treatments (A), base materials (B), morphologies (C), physico-chemical properties and toxicological endpoints (D), respectively. The heatmaps are colored according to the correlation and significance of correlation is indicated (*: p-value ≤ 0.1, **: p-value ≤ 0.05, ***: p-value ≤ 0.01).

Silica-specific effects

In the present study three silica NMs with different sizes and synthesis routes (pyrogenic and precipitated) were investigated. Hence, silica-specific effects were analyzed. Silica was the only core material that positively correlated with the turquoise module (Figure 3B), with enrichment of mitochondrial dysfunction, DNA damage response and cell death (Table S11). Furthermore, significant negative correlation was observable for modules with enriched central carbon metabolism, ERK/MAPK signaling, NRF2-mediated oxidative stress response and cytokine signaling.

Physico-chemical properties

Next, we aimed to correlate alterations in proteome and metabolome of NR8383 cells with physico-chemical properties to get hints into the property-activity relationship. Most significant correlations were found for agglomerate size, showing positive correlation with cytokine signaling, phagocytosis, NRF2-mediated oxidative stress response and mitochondrial dysfunction.

DMPO reactivity showed significant correlations with the red and grey modules. The correlation pattern was similar to the one observed for Mn2O3 (Figure 3A), suggesting that changes could be Mn2O3-specific, according to its high oxidative potential (Delaval *et al.*, 2017). Importantly, no significant correlation was observed with the surface area corrected DMPO reactivity, indicating that their reactivity is mainly determined by the available surface area.

The band gap showed significant correlation with ERK/MAPK Signaling and NRF2-mediated oxidative stress response for instance (magenta module). NMs positively correlating with this module (Figure 3A) were Graphene Oxide, Phthalocyanine Blue and Phthalocyanine Green, suggesting this module to be specific for these NMs.

Toxicological endpoints

From the toxicological endpoints, LDH release led to most significant correlations. This parameter showed a negative correlation with the agglomerate size, indicating that NMs such as SiO2_15, SiO2_7 and SiO2_40 forming small agglomerates led to higher LDH release, and hence low cell viability.

TNFα release showed significant positive correlation with analytes related to NRF2-mediated oxidative stress response and chemokine signaling. Furthermore, significant negative correlations were observed for production of nitric oxide and reactive oxygen species in macrophages and cell death. Interestingly, TNFα release clustered with LDH release.

Key driver analysis

To identify key drivers involved in the NMs MoA, we determined analytes highly connected to particular modules and traits (e.g. silica, surface area, LDH or TNFα release), suggesting their importance as mediators of the observed effects (Figure 4). The list of key drivers (Figure 5) comprises proteins from different pathways and different biological functions ranging from immune response to DNA damage (Table S12). Taken together, all of them allowed distinguishing between the tested silica NMs and the others, with the exception of Mn2O3.

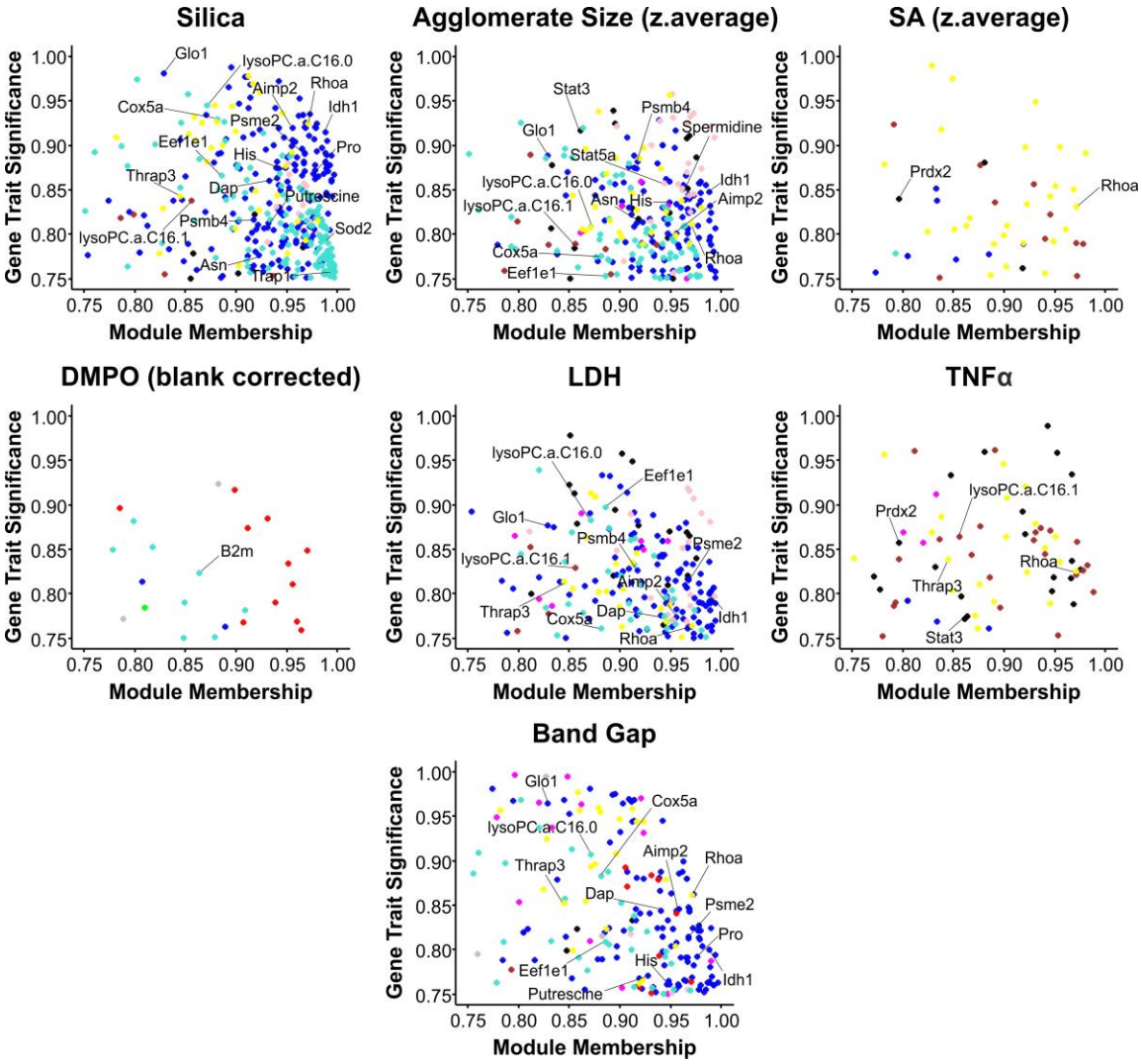

Figure 4: Identified key drivers.
Plotted are analytes with absolute gene significance ≥ 0.75 and absolute module membership ≥ 0.75 for traits highly correlating with at least one module. Analytes are colored based on their assigned module.

Especially Idh1 and Sod2 allowed the differentiation of SiO2_7, SiO2_15 and SiO2_40 from both phthalocyanines and Graphene Oxide. In these cases, Mn2O3 showed similar behavior as the silica NMs but with less intensity. Interestingly, Idh1 and Sod2 are both related to oxidative stress, which is consistent with the observation that oxidative stress is one of the most common routes upon NM treatment (Lujan and Sayes, 2017).

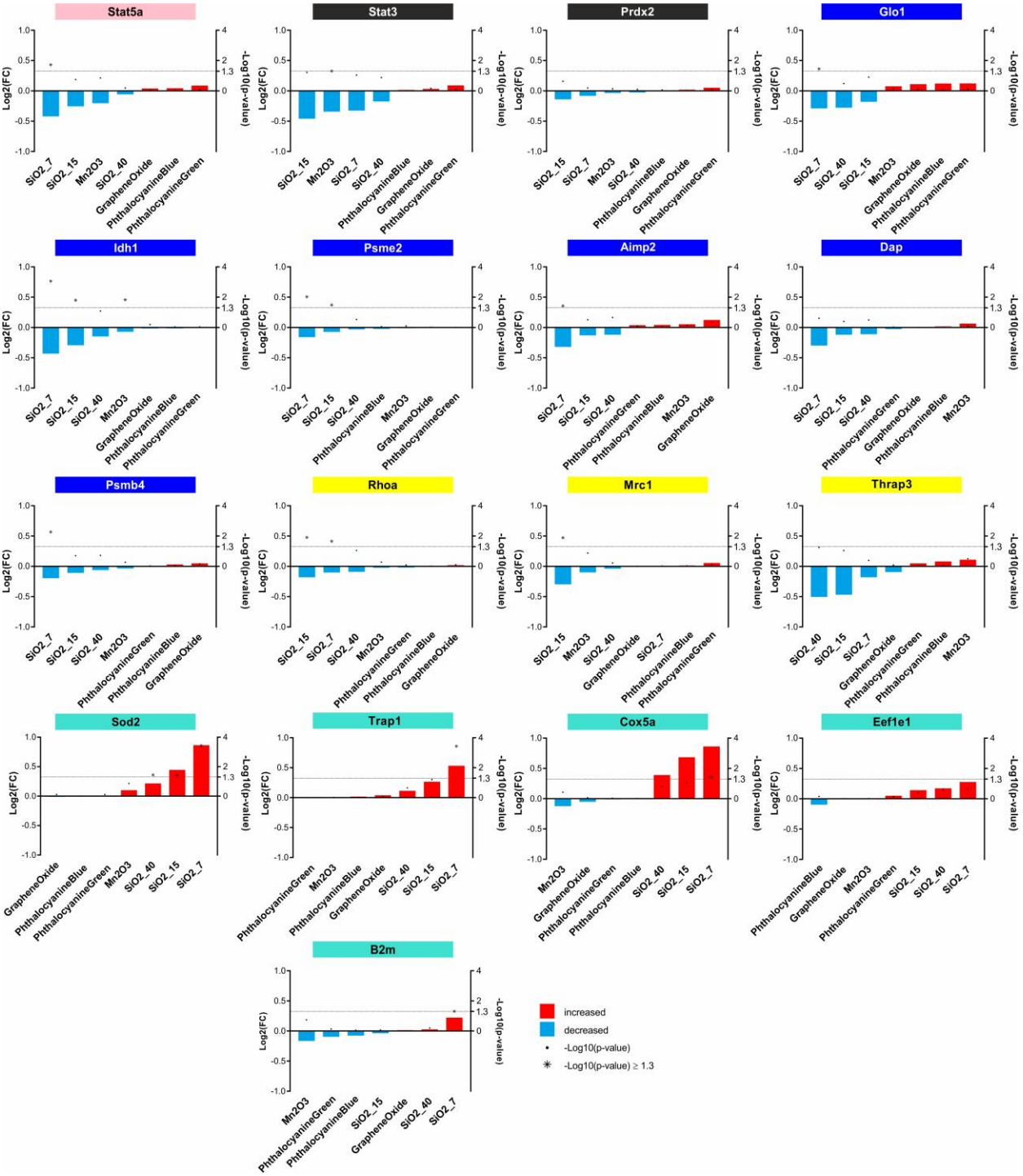

Figure 5: Proteins that were identified to be key drivers.
Shown are protein Log2(FCs) (left axis) and p-values (right axis) with respect to the control. Significantly (p-value ≤ 0.05) altered proteins are highlighted (*). Furthermore, assigned modules are indicated by the color behind the analyte name.

Metabolites suggested to be key drivers are shown in Figure 6. Interestingly, most metabolites clearly separated the supposedly "active" silica NMs from others, again with exception of Mn2O3.

Relevant molecules were lysoPC.a.C.16.0 and lysoPC.a.C.16.1 (phosphatidylcholines), Asn, His and Pro (amino acids), spermidine and putrescine (biogenic amines).

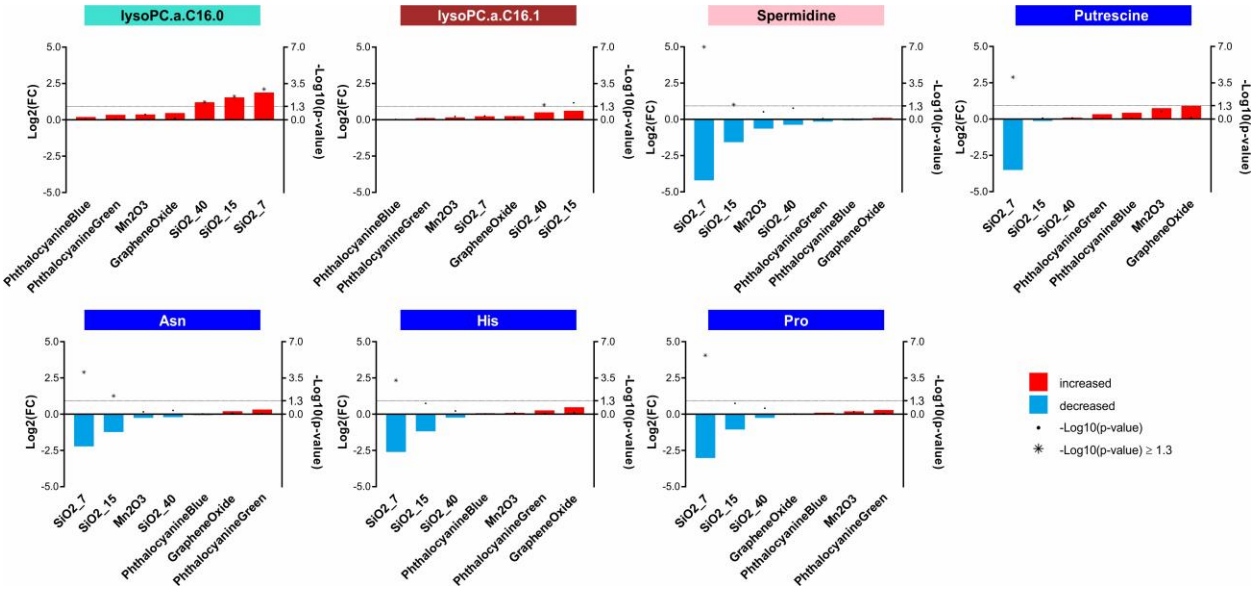

Figure 6: Metabolites that were identified to be key drivers.
Shown are metabolite Log2(FCs) (left axis) and p-values (right axis) with respect to the control. Significantly (p-value ≤ 0.05) altered metabolites are highlighted (*). Furthermore, assigned modules are indicated by the color behind the analyte name.

Dose dependency

To get deeper insights into dose-dependent effects, the silica NMs were assessed at 2.5, 5 and 10 µg/cm^2 using proteomics and metabolomics. The dose-dependent abundances for several key drivers that were initially identified based on the screening (Figures 5 and 6) indicate that SiO2_7 induced the highest concentration-dependent responses, followed by SiO2_15 and SiO2_40 (Figure 7). This is true for spermidine as well as several proteins. Especially Sod2, B2m, Thrap3 and Trap1 showed concentration dependencies, which confirms the findings from the screening and renders them interesting biomarkers candidates. Thus, several key drivers, that confirm the separation of “active” NMs from “passive” NMs, were identified, which might facilitate future risk assessment. The dose-dependent effects for the three silica NMs were also investigated by the

assessment of toxicological endpoints (Table S10) that showed dose-dependent signals as well. Thereby, the highest response was achieved by SiO2_7, followed by SiO2_15 and SiO2_40, which is in accordance with the obtained results for the key drivers.

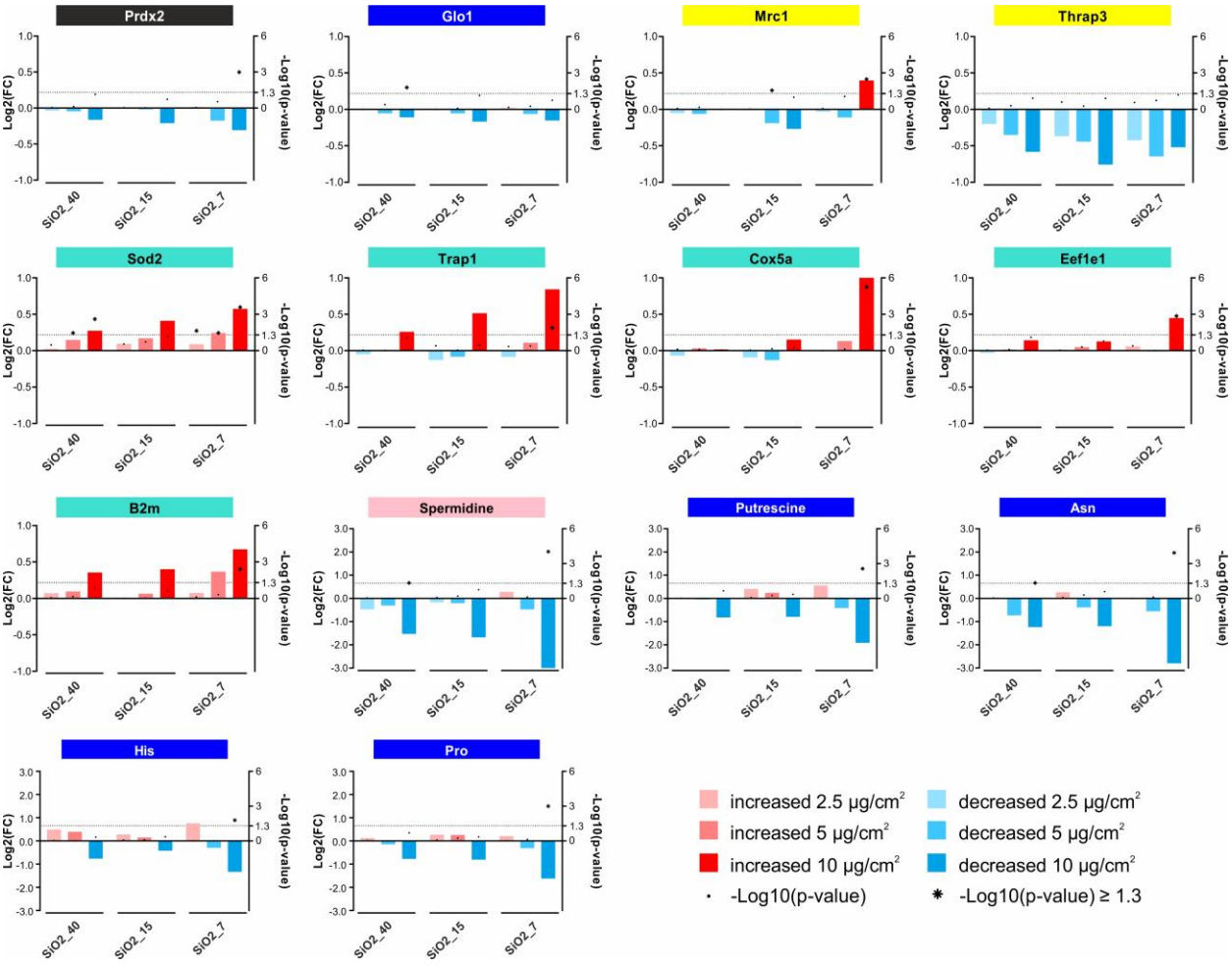

Figure 7: Concentration dependency of selected key drivers.
Shown are Log2(FCs) (left axis) and p-values (right axis) for selected key drivers that were extracted from data obtained by applying proteomics and metabolomics with different NM doses. Significantly (p-value ≤ 0.05) altered analytes are highlighted (*). Furthermore, assigned modules are indicated by the color behind the analyte name.

Discussion

A detailed understanding of NM toxicity mechanisms and NM MoAs is useful for the distinction and/or grouping of NMs. Here we applied a multi-omics approach including proteomics, SH2 profiling and metabolomics to a set of seven NMs with different properties. Interestingly, all three omics approaches led to similar outcomes with respect to NM categorization, indicating the reliability of our approach. Moreover, the integrative hierarchical clustering analysis of this multi-omics data set (Figure 2) gave a refined view with respect to the existing classification into “active” and “passive” NMs, confirming SiO2_7, SiO2_15 and SiO2_40 to be “active” *in vitro*. This classification was also supported by the analysis of key drivers and toxicological endpoints in the concentration-dependent follow-up studies. Based on the data of the four toxicological endpoints (Table S10), these particles were all to be classified as "active" according to the existing classification, under consideration of the NMs surface areas. SiO2_15 has been shown to be “active” *in vitro* (Wiemann *et al.*, 2016) and *in vivo* (Landsiedel *et al.*, 2014) before, which is consistent with our findings.

Phthalocyanine Blue, Phthalocyanine Green and Graphene Oxide showed almost no changes, suggesting them to be “passive” *in vitro*. Phthalocyanine Blue has been shown before to be “active” *in vitro* (Wiemann *et al.*, 2016) and “passive” *in vivo* (Landsiedel *et al.*, 2014, Arts *et al.*, 2016), showing that a more detailed investigation as done here can support the previous *in vivo* observations even though simple toxicity assessment in the same cell model has suggested that this NM can be “active”, which is an additional evidence that the MoA should be considered to establish NM grouping.

When taking together all evidences, Mn2O3 should be classified as “active” as well. While it did not induce significant changes in the metabolome, there were significant changes observable in the proteome. Furthermore, it was located between the supposedly “active” and “passive” materials within the WGCNA (Figure 3A) and in case of several of the key drivers the abundances had the same direction as in case of the NMs that were classified to be “active” within this study. Examples are Stat5a, Stat3, Idh1, and Sod2 (Figure 5). Nevertheless, we would have expected stronger and more pronounced effects for Mn2O3 since this material has already been described as cytotoxic and inducing high cellular oxidative stress levels (Zhang *et al.*, 2012, Hsieh *et al.*, 2013). This was not the case in this study. However, differences in NM dispersion methods resulting in differences in agglomerate sizes or differences in cell treatment may account for these variations and need further investigations.

The integrative analysis of the results from proteomics and metabolomics in this study was conducted using WGCNA, that allows not only the identification of relevant physico-chemical properties or toxicological endpoints but also to unravel key drivers that are highly connected to particular traits, thus rendering them representative biomarker candidates for future NM toxicity assessment. The conducted key driver analysis revealed several interesting candidates. On the proteome level especially the proteins that are related to oxidative stress response or mitochondrial dysfunction (e.g. Sod2, Cox5a) allow to distinguish the supposedly “active” NMs from the others and show concentration dependencies. However, most of the other identified proteins did not show significant (p-value ≤ 0.05) changes in protein abundances for all the supposedly “active” NMs, which makes categorization based on these data alone challenging. Importantly, there were also several metabolites identified to be key drivers, from which especially phosphatidylcholines, amino acids and biogenic amines seem to be suitable to distinguish “active” and “passive” NMs.

In summary, consistent results for a systematically selected set of NMs were obtained within this multi-omics approach, revealing important insights into potential toxicity mechanisms, including immune responses, oxidative stress response and cell death, which is in accordance with the literature (Li et al., 2008). Furthermore, our study identified physico-chemical properties that can be correlated with observed effects, which allowed distinguishing supposedly "active" from "passive" NMs. Finally, we identified biomarker candidates that might facilitate future hazard and risk assessment.

Conclusions

In this study, a set of seven different NMs was investigated, including three silica NMs with varying properties. Biological effects were identified using a multi-omics approach with untargeted proteomics, SH2 profiling and targeted metabolomics. Interestingly, all conducted hierarchical clustering analyses revealed overall similar categorization outcomes, showing that results from different omics data sets were highly consistent. The integrative hierarchical clustering analysis involving all three data sets was the most predictive one in terms of the classification confirming that more parameters allow a more reliable categorization. The conducted WGCNA was a valuable tool to assess NM toxicity since it revealed insights into the NMs MoAs and unraveled physico-chemical properties that were related to observed effects. Furthermore, key drivers were identified based on WGCNA results that might be representative biomarkers for future risk assessment. While metabolites and phosphoproteins where shown to be already suitable indicators of NM toxicity, the proteome is necessary to unravel MoAs due to the information about key events and regulated pathways. In summary, the obtained insights may be useful for future approaches to facilitate targeted hazard and risk assessment and grouping.

Disclosure of Interest

The authors report no conflict of interest.

Funding

This project is part of the SIINN ERA-NET and is funded under the ERA-NET scheme of the Seventh Framework Program of the European Commission, BMBF Grant Agreement No. 03XP0008.

Acknowledgements

The authors would like to take this opportunity to thank all institutions for their support of this project. In addition, the authors want to thank Antje Bergert and Doreen Wittke for excellent technical assistance.

Data availability statement

The proteomics and metabolomics datasets generated in this study are available at Zenodo under following DOI: https://doi.org/10.5281/zenodo.3514213.

References

Arts, J.H., Hadi, M., Irfan, M.-A., Keene, A.M., Kreiling, R., Lyon, D., Maier, M., Michel, K., Petry, T. & Sauer, U.G., 2015. A decision-making framework for the grouping and testing of nanomaterials (DF4nanoGrouping). *Regulatory Toxicology and Pharmacology,* 71**,** S1-S27.

Arts, J.H., Irfan, M.A., Keene, A.M., Kreiling, R., Lyon, D., Maier, M., Michel, K., Neubauer, N., Petry, T., Sauer, U.G., Warheit, D., Wiench, K., Wohlleben, W. & Landsiedel, R., 2016. Case studies putting the decision-making framework for the grouping and testing of nanomaterials (DF4nanoGrouping) into practice. *Regul Toxicol Pharmacol,* 76**,** 234-61.

Delaval, M., Wohlleben, W., Landsiedel, R., Baeza-Squiban, A. & Boland, S., 2017. Assessment of the oxidative potential of nanoparticles by the cytochrome c assay: assay improvement and development of a high-throughput method to predict the toxicity of nanoparticles. *Arch Toxicol,* 91**,** 163-177.

Dierck, K., Machida, K., Mayer, B.J. & Nollau, P., 2009. Profiling the tyrosine phosphorylation state using SH2 domains. *Phospho-Proteomics.* Springer, 131-155.

Donaldson, K., Aitken, R., Tran, L., Stone, V., Duffin, R., Forrest, G. & Alexander, A., 2006. Carbon nanotubes: a review of their properties in relation to pulmonary toxicology and workplace safety. *Toxicol Sci,* 92**,** 5-22.

Dong, J. & Ma, Q., 2015. Advances in mechanisms and signaling pathways of carbon nanotube toxicity. *Nanotoxicology,* 9**,** 658-676.

Driessen, M.D., Mues, S., Vennemann, A., Hellack, B., Bannuscher, A., Vimalakanthan, V., Riebeling, C., Ossig, R., Wiemann, M. & Schnekenburger, J., 2015. Proteomic analysis of protein carbonylation: a useful tool to unravel nanoparticle toxicity mechanisms. *Particle and Fibre Toxicology,* 12**,** 36.

Feliu, N., Pelaz, B., Zhang, Q., Del Pino, P., Nystrom, A. & Parak, W.J., 2016. Nanoparticle dosage-a nontrivial task of utmost importance for quantitative nanosafety research. *Wiley Interdiscip Rev Nanomed Nanobiotechnol,* 8**,** 479-92.

Gallud, A., Klöditz, K., Ytterberg, J., Östberg, N., Katayama, S., Skoog, T., Gogvadze, V., Chen, Y.-Z., Xue, D., Moya, S., Ruiz, J., Astruc, D., Zubarev, R., Kere, J. & Fadeel, B., 2019. Cationic gold nanoparticles elicit mitochondrial dysfunction: a multi-omics study. *Scientific Reports,* 9**,** 4366.

Gerloff, K., Landesmann, B., Worth, A., Munn, S., Palosaari, T. & Whelan, M., 2017. The Adverse Outcome Pathway approach in nanotoxicology. *Computational Toxicology,* 1**,** 3-11.

Hsieh, S.F., Bello, D., Schmidt, D.F., Pal, A.K., Stella, A., Isaacs, J.A. & Rogers, E.J., 2013. Mapping the biological oxidative damage of engineered nanomaterials. *Small,* 9**,** 1853-65.

Hughes, C.S., Foehr, S., Garfield, D.A., Furlong, E.E., Steinmetz, L.M. & Krijgsveld, J., 2014. Ultrasensitive proteome analysis using paramagnetic bead technology. *Mol Syst Biol,* 10**,** 757.

Hughes, C.S., Moggridge, S., Muller, T., Sorensen, P.H., Morin, G.B. & Krijgsveld, J., 2018. Single-pot, solid-phase-enhanced sample preparation for proteomics experiments. *Nat Protoc*.

Kroll, A., Dierker, C., Rommel, C., Hahn, D., Wohlleben, W., Schulze-Isfort, C., Göbbert, C., Voetz, M., Hardinghaus, F., Schnekenburger, J.J.P. & Toxicology, F., 2011. Cytotoxicity screening of 23 engineered nanomaterials using a test matrix of ten cell lines and three different assays. 8**,** 9.

Krug, H.F., 2014. Nanosafety Research—Are We on the Right Track? *Angewandte Chemie International Edition,* 53**,** 12304-12319.

Landsiedel, R., Fabian, E., Ma-Hock, L., Van Ravenzwaay, B., Wohlleben, W., Wiench, K. & Oesch, F., 2012. Toxico-/biokinetics of nanomaterials. *Arch Toxicol,* 86**,** 1021-60.

Landsiedel, R., Ma-Hock, L., Hofmann, T., Wiemann, M., Strauss, V., Treumann, S., Wohlleben, W., Groters, S., Wiench, K. & Van Ravenzwaay, B., 2014. Application of short-term inhalation studies to assess the inhalation toxicity of nanomaterials. *Part Fibre Toxicol,* 11**,** 16.

Langfelder, P. & Horvath, S., 2008. WGCNA: an R package for weighted correlation network analysis. *BMC Bioinformatics,* 9**,** 559.

Li, N., Xia, T. & Nel, A.E., 2008. The role of oxidative stress in ambient particulate matter-induced lung diseases and its implications in the toxicity of engineered nanoparticles. *Free radical biology and medicine,* 44**,** 1689-1699.

Lin, Z., Ma, L., X, Z.G., Zhang, H. & Lin, B., 2013. A comparative study of lung toxicity in rats induced by three types of nanomaterials. *Nanoscale Res Lett,* 8**,** 521.

Louro, H., 2018. Relevance of Physicochemical Characterization of Nanomaterials for Understanding Nano-cellular Interactions. *Adv Exp Med Biol,* 1048**,** 123-142.

Love, M.I., Huber, W. & Anders, S., 2014. Moderated estimation of fold change and dispersion for RNA-seq data with DESeq2. *Genome biology,* 15**,** 550.

Lujan, H. & Sayes, C.M., 2017. Cytotoxicological pathways induced after nanoparticle exposure: studies of oxidative stress at the 'nano-bio' interface. *Toxicol Res (Camb),* 6**,** 580-594.

Mcshan, D., Ray, P.C. & Yu, H., 2014. Molecular toxicity mechanism of nanosilver. *J Food Drug Anal,* 22**,** 116-127.

Nath Roy, D., Goswami, R. & Pal, A., 2017. Nanomaterial and toxicity: what can proteomics tell us about the nanotoxicology? *Xenobiotica,* 47**,** 632-643.

Nel, A., Xia, T., Mädler, L. & Li, N., 2006. Toxic potential of materials at the nanolevel. *science,* 311**,** 622-627.

Oberdörster, G., Oberdörster, E. & Oberdörster, J., 2005. Nanotoxicology: an emerging discipline evolving from studies of ultrafine particles. *Environ Health Perspect,* 113**,** 823-39.

Oecd, 2012. *Proposal for a template and guidance on developing and assessing the completeness of adverse outcome pathways*.

Oecd, 2018. *REPORT ON CONSIDERATIONS FROM CASE STUDIES ON INTEGRATED APPROACHES FOR TESTING AND ASSESSMENT (IATA), ENV/JM/MONO(2018)25, Series on Testing and Assessment No. 289*.

Olson, H., Betton, G., Robinson, D., Thomas, K., Monro, A., Kolaja, G., Lilly, P., Sanders, J., Sipes, G., Bracken, W., Dorato, M., Van Deun, K., Smith, P., Berger, B. & Heller, A., 2000. Concordance of the Toxicity of Pharmaceuticals in Humans and in Animals. *Regulatory Toxicology and Pharmacology,* 32**,** 56-67.

Pei, G., Chen, L. & Zhang, W., 2017. WGCNA Application to Proteomic and Metabolomic Data Analysis. *Methods Enzymol,* 585**,** 135-158.

Potratz, S., Tarnow, P., Jungnickel, H., Baumann, S., Von Bergen, M., Tralau, T. & Luch, A., 2017. Combination of Metabolomics with Cellular Assays Reveals New Biomarkers and Mechanistic Insights on Xenoestrogenic Exposures in MCF-7 Cells. *Chemical Research in Toxicology*.

Rahi, A., Sattarahmady, N. & Heli, H., 2014. Toxicity of Nanomaterials-Physicochemical Effects. *Austin J Nanomed Nanotechnol,* 2**,** 1034-1042.

Riebeling, C., Jungnickel, H., Luch, A. & Haase, A., 2017. Systems Biology to Support Nanomaterial Grouping. *Adv Exp Med Biol,* 947**,** 143-171.

Sandberg, A., Branca, R.M.M., Lehtiö, J. & Forshed, J., 2014. Quantitative accuracy in mass spectrometry based proteomics of complex samples: The impact of labeling and precursor interference. *Journal of Proteomics,* 96**,** 133-144.

Scala, G., Kinaret, P., Marwah, V., Sund, J., Fortino, V. & Greco, D., 2018. Multi-omics analysis of ten carbon nanomaterials effects highlights cell type specific patterns of molecular regulation and adaptation. *NanoImpact,* 11**,** 99-108.

Shanks, N., Greek, R. & Greek, J., 2009. Are animal models predictive for humans? *Philosophy, ethics, and humanities in medicine : PEHM,* 4**,** 2-2.

Shatkin, J.A. & Ong, K.J., 2016. Alternative Testing Strategies for Nanomaterials: State of the Science and Considerations for Risk Analysis. 36**,** 1564-1580.

Stark, W.J., Stoessel, P.R., Wohlleben, W. & Hafner, A.J.C.S.R., 2015. Industrial applications of nanoparticles. 44**,** 5793-5805.

Taurozzi, J.S., Hackley, V.A. & Wiesner, M.R., 2011. Ultrasonic dispersion of nanoparticles for environmental, health and safety assessment--issues and recommendations. *Nanotoxicology,* 5**,** 711-29.

Tee, J.K., Ong, C.N., Bay, B.H., Ho, H.K. & Leong, D.T., 2016. Oxidative stress by inorganic nanoparticles. 8**,** 414-438.

Thompson, A., Schafer, J., Kuhn, K., Kienle, S., Schwarz, J., Schmidt, G., Neumann, T., Johnstone, R., Mohammed, A.K. & Hamon, C., 2003. Tandem mass tags: a novel

quantification strategy for comparative analysis of complex protein mixtures by MS/MS. *Anal Chem,* 75**,** 1895-904.

Wall, R.J. & Shani, M., 2008. Are animal models as good as we think? *Theriogenology,* 69**,** 2-9.

Wewering, F., Jouy, F., Wissenbach, D.K., Gebauer, S., Blüher, M., Gebhardt, R., Pirow, R., Von Bergen, M., Kalkhof, S. & Luch, A., 2016. Characterization of chemical-induced sterile inflammation in vitro: application of the model compound ketoconazole in a human hepatic co-culture system. *Archives of toxicology***,** 1-12.

Wiemann, M., Vennemann, A., Sauer, U.G., Wiench, K., Ma-Hock, L. & Landsiedel, R., 2016. An in vitro alveolar macrophage assay for predicting the short-term inhalation toxicity of nanomaterials. *J Nanobiotechnology,* 14**,** 16.

Wiemann, M., Vennemann, A., Stintz, M., Retamal Marin, R.R., Babick, F., Lindner, G.G., Schuster, T.B., Brinkmann, U. & Krueger, N., 2018. Effects of Ultrasonic Dispersion Energy on the Preparation of Amorphous SiO(2) Nanomaterials for In Vitro Toxicity Testing. *Nanomaterials (Basel),* 9.

Xia, T., Hamilton, R.F., Bonner, J.C., Crandall, E.D., Elder, A., Fazlollahi, F., Girtsman, T.A., Kim, K., Mitra, S., Ntim, S.A., Orr, G., Tagmount, M., Taylor, A.J., Telesca, D., Tolic, A., Vulpe, C.D., Walker, A.J., Wang, X., Witzmann, F.A., Wu, N., Xie, Y., Zink, J.I., Nel, A. & Holian, A., 2013. Interlaboratory evaluation of in vitro cytotoxicity and inflammatory responses to engineered nanomaterials: the NIEHS Nano GO Consortium. *Environ Health Perspect,* 121**,** 683-90.

Zhang, B. & Horvath, S., 2005. A general framework for weighted gene co-expression network analysis. *Stat Appl Genet Mol Biol,* 4**,** Article17.

Zhang, H., Ji, Z., Xia, T., Meng, H., Low-Kam, C., Liu, R., Pokhrel, S., Lin, S., Wang, X., Liao, Y.P., Wang, M., Li, L., Rallo, R., Damoiseaux, R., Telesca, D., Madler, L., Cohen, Y., Zink, J.I. & Nel, A.E., 2012. Use of metal oxide nanoparticle band gap to develop a predictive paradigm for oxidative stress and acute pulmonary inflammation. *ACS Nano,* 6**,** 4349-68.

Additional Files

Reference	File name	Description
Additional file 1	Additional file 1.xlsx	Replicate values, FCs and p-values obtained from proteomics, metabolomics and SH2 profiling.
Additional file 2	Additional file 2.xlsx	Scaled data from proteomics and metabolomics that were used for WGCNA.
Additional file 3	Additional file 3.xlsx	Lists of analytes and their assignment to obtained modules.
Additional file 4	Additional file 4.xlsx	Summary of enriched pathway for each module.
Additional file 5	Additional file 5.xlsx	Calculated module memberships and gene significances together with identified key drivers.
Supplement	Supplement.pdf	All tables and figures that were mentioned to be in the Supplement within the text.